Hydroxypropyl cellulose as fluorine-free alternative binder for aqueous supercapacitors

Journal of Energy Storage 131 (2025) 117532

Contents lists available at ScienceDirect

Journal of Energy Storage

journal homepage: www.elsevier.com/locate/est

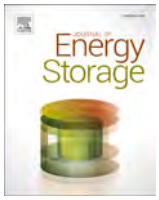

Research papers

Hydroxypropyl cellulose as fluorine-free alternative binder for aqueous supercapacitors

Simone Martellone [a,b], Davide Molino [a], Davide Arcoraci [a], Giorgio Mogli [a], Mara Serrapede [a], Giuseppe Ferraro [a], Alessandro Pedico [a,c], Sergio Bocchini [a,b], Pietro Zaccagnini [a,b,*], Andrea Lamberti [a,b]

[a] Dipartimento di scienze applicate e tecnologia – Politecnico di Torino, Corso Duca degli Abruzzi 24, 10129 Torino, Italy
[b] Centre for Sustainable and Future Technologies – Istituto Italiano di Tecnologia, Via Livorno 60, 10144 Torino, Italy
[c] Istituto Nazionale di Ricerca Metrologica (INRiM), Strada delle Cacce 91, 10135, Torino, Italy

ARTICLE INFO

Keywords:
Supercapacitor
Fluorine-free
Cellulose binder
Aqueous device
Sustainability

ABSTRACT

The development of sustainable energy storage devices, such as supercapacitors (SCs), pushes towards innovative material science solutions. This study presents Hydroxypropyl Cellulose (HPC) as a promising fluorine-free binder (FFB) alternative to traditional fluorinated binders exploited in aqueous-based electrolytic systems. HPC offers water solubility and pH stability, making it an environmentally friendly option for aqueous electrolyte-based SCs. We investigated HPC's efficacy as a binder in activated carbon-based SC electrodes due to its *salt out effect*, comparing it with conventional Polyvinylidene Fluoride (PVDF) binder. Electrodes were tested in acidic (1 N H_2SO_4), neutral (1 N Na_2SO_4), and basic (1 N *KOH*) electrolytes, with titanium current collectors. Our findings reveal that HPC-based electrodes exhibit superior uniformity and interconnectivity, as evidenced by electron microscopy and surface area measurements. Electrochemical characterizations demonstrate that HPC electrodes outperform PVDF counterparts in all tested electrolytes, particularly in terms of chemical stability in basic solutions where PVDF degrades. The HPC devices achieved specific capacitances of 22.21 F g^{-1} (acidic), 17.03 F g^{-1} (neutral), and 23.86 F g^{-1} (basic) with over 90 % retention after 10,000 charge-discharge cycles and 160 h of floating tests. These results suggest that HPC not only ensures environmental safety but also enhances performance and durability across various pH environments. In conclusion, HPC proved to be a sustainable and effective binder for electrochemical systems with both capacitive and faradic electrodes. Future research should focus on integrating HPC with more stable current collectors to further improve devices' performance, especially in acidic media, seawater and wastewater, thus advancing the field of eco-friendly energy storage technologies.

1. Introduction

In the relentless pursuit of sustainable energy solutions, the quest for high-performance energy storage devices has never been more critical. From portable electronics to electric vehicles and grid-scale storage systems, the efficiency and reliability of these devices are pivotal for advancing renewable energy integration and mitigating climate change. In this direction, the significance of fluorine-free energy storage systems cannot be overstated [1–3]. To date, the most investigated and developed electrical energy storage systems are supercapacitors (SCs) and batteries, and their hybrid forms referred to as hybrid capacitors (HCs) [4]. SCs feature high power densities and low energy densities, while batteries are complementing such characteristics featuring high energy densities and low power capabilities. HCs represent a trending research and industry development field since they feature both high energy and power densities [5–8]. All these devices share similar fabrication procedures, concerning the electrodes: the active material is wet processed in an ink and coated over a current collector substrate. One of the ink elements is the binder with the main purpose to promote ink adhesion in the dried state over the current collector, cohesion of the active material particles and overall mechanical stability in a roll-to-roll (R2R) process. At present, fluorinated binders have not been completely removed. Moreover, they require toxic solvents to be dissolved and processed such as N-Methyl Pyrrolidone (NMP). These polymers, like polyvinylidene fluoride (PVDF) and polytetrafluoroethylene (PTFE), are still widely used in aqueous electrolyte systems since they do not dissolve in water

* Corresponding author at: Dipartimento di scienze applicate e tecnologia – Politecnico di Torino, Corso Duca degli Abruzzi 24, 10129 Torino, Italy.
E-mail address: pietro.zaccagnini@polito.it (P. Zaccagnini).

https://doi.org/10.1016/j.est.2025.117532
Received 1 March 2025; Received in revised form 21 May 2025; Accepted 21 June 2025
Available online 1 July 2025

[9–13].

Fluorine-based binders have traditionally been favored for their adhesive properties and chemical stability. However, concerns over environmental impact and health hazards associated with fluorine compounds have prompted a paradigm shift towards fluorine-free alternatives. One of the primary advantages of fluorine-free binders (FFBs) lies in their environmental friendliness. Unlike fluorine-based counterparts, which pose risks of bioaccumulation and toxicity [14–16], FFBs present minimal environmental impact throughout their lifecycle [17,18]. By eliminating fluorine from the binder composition, the production, application, and disposal phases of energy storage devices can be made more sustainable, aligning with the principles of circular economy and responsible manufacturing practices.

Moreover, the absence of fluorine in binders enhances safety in manufacturing processes. Fluorine compounds, particularly perfluorinated substances, are notorious for their inflammability and hazardous by-products when exposed to high temperatures. By opting for FFBs, manufacturers reduce the likelihood of accidents and minimize occupational health risks, in view of a safer working environment.

In the field of Fuel Cells and Electrolyzers, the discussion around chemical stability is relevant, with particular emphasis on the Fluoride Emission Rate (FER) [19–21]. In these systems, fluoropolymers such as Nafion are also used as binder [22–30]. This metric (FER) is crucial, not only for assessing the operational longevity and safety of these systems, but also because of its broader implications for environmental sustainability. Interestingly, the concern with fluoride emissions might extend into the domain of supercapacitors, where fluoropolymers are employed as binders, as well as in capacitive de-ionization systems [31–34]. These materials, while enhancing the chemical stability in water environment of SC electrodes, also pose a risk of fluoride emission, thereby connecting the discussions on chemical stability. For these reasons, moving towards fluorine-free systems is advisable.

Furthermore, FFBs exhibit superior electrochemical performance, crucial for the efficiency and longevity of energy storage devices [35–37]. These binders offer enhanced ion conductivity and mechanical stability, facilitating better electrode adhesion and minimizing electrode degradation over cycles [38–40]. Consequently, energy storage devices utilizing FFBs demonstrate improved energy density, cycle life, and overall performance, translating into enhanced reliability and cost-effectiveness.

The transition towards FFBs is not without challenges. Researchers face the task of developing formulations that match or exceed the performance metrics of fluorine-based counterparts while maintaining cost competitiveness. Additionally, ensuring scalability and compatibility with existing manufacturing processes remains a priority to facilitate widespread adoption. Therefore, the adoption of FFBs represents a pivotal step towards sustainable and high-performance energy storage devices. Beyond addressing environmental and health concerns, these binders unlock opportunities for innovation, efficiency, and safety across the energy storage value chain. In a recent work of Li et al., a cellulose-based binder, Hydroxyethyl Cellulose (HEC) has been demonstrated as a functional co-binder for high mass loading cathodes enhancing the overall mechanical properties [41].

Enhancing the mass loading of electrodes is particularly in the field of SCs, in particular HCs. The development of porous carbon materials with tailored structures and heteroatom doping has gained significant attention for application in SCs and HCs, due to the promising results in terms of specific capacitance. Recycling of sources such as waste tire pyrolysis oil (WTPO) [42,43], biomasses [44] and coal pitch [45] to produce advanced materials with enhanced performance metrics. Trends in porous carbon S and N doping and co-doping are observed [45–52] providing enhanced performances. Incorporating these materials into high loading electrodes, for HCs application, and low loading electrodes, for EDLC applications, is of interest if sustainable binder solutions are used like the commercially available Acrylonitrile multicopolymer binder (LA1333).

The present work discusses the study in the application of a synthetic non-ionic cellulose to water-based electrolyte SC, namely Hydroxypropyl Cellulose (HPC). HPC is a synthetic derivative of the most abundant natural polymer on Earth crust, natural cellulose (NC). HPC is obtained from NC by adding hydroxypropyl groups on cellulose via etherification process. The HPC monomer structure is depicted in Fig. S1, compared to the one of NC. Moreover, in a recent work, Joshi et al. proven waste papers a promising feedstock for HPC synthesis offering an environmentally friendly approach for waste reduction and management [53]. Also, HPC synthesis was proved to be feasible from bacterial cellulose in the work of Chen et al. [54]

A direct consequence of the abundance of NC on Earth, is that the cost of its derivatives, such as HPC and CMC, are significantly less expensive than fluorine-based materials like PVDF, Nafion, or PTFE. This cost difference arises from the more complex and expensive production processes required for fluoropolymers. According to various studies, cellulose-based binders are roughly an order of magnitude cheaper than their fluorine-based counterparts. For instance, PVDF typically costs around $10–15 per kilogram, while carboxymethyl cellulose (CMC), the most common cellulose-based binder, costs approximately $2–4 per kilogram [17,55–58]. Specifically, in the context of this study, PVDF is priced at about $14 per kilogram, whereas HPC is estimated at $4 per kilogram.

Thanks to the etherification process, HPC has the unique property of being soluble in both water and organic solvents [59,60]. At temperatures above 38 °C and lower than 0 °C, HPC is no more soluble in water solution and already dissolved chains start precipitating. This flocculation is thermally reversible. Furthermore, HPC does not significantly alter the pH as dissolved in water solution and it is stable in water solution in a wide range of pH from 2 to 11. In contrast to methylated celluloses, HPC never forms a gel, not even under the addition of gelling agents. The rheological behavior of HPC based solutions changes if mixed with alcohols, especially ethanol (EtOH). Usually, the presence of other substances in water-based solutions of HPC mainly impacts the cloud point. In the case of alcohol such as EtOH, these solutions can be heated up to the boiling point without flocculation. Solution clouding, precipitation, no dissolution can happen in the presence of other substances, especially when concentrated, because there is not enough solvent to keep HPC in a hydrated state. In extremely concentrated solutions, HPC molecule precipitates in the solution in an extremely swollen product in a process called salting-out. The ‘salting-out effect’ is defined as the separation of an organic phase from an aqueous phase by adding a salt [61]. For these reasons, we selected HPC as a suitable binder for aqueous processable inks for aqueous electrolyte-based supercapacitor.

Among the different work on natural polymers for energy storage devices [56,62–64], and bio-derived polymers [65], HPC has been reported in the work of Sun et al. as binder agent for 3D printed batteries working in organic electrolyte [66]. In the field of batteries, HPC has also been proposed as functional binder in lithium-sulfur systems [67]. Also, hydroxypropyl methyl cellulose (HPMC), a slightly different variation of HPC, has been employed as binding agent for 3D printed devices working in aqueous electrolyte [68].

With respect to the state-of-the-art Sodium Carboxymethyl cellulose (CMC), HPC is also immune from microbial attack. Being an ionic compound, CMC is not suitable for water-based energy storage devices since the interaction of CMC with monovalent ions does not produce any flocculation, causing possible dissolution of the binder and electrodes’ degradation. Compared to the other popular FFBs, HPC does not require any additional processing thanks to its salting out effect. In contrast, other commonly used binders such as chitosan and sodium alginate typically require an additional cross-linking step to ensure stability in water-based environments [69,70]. This simplifies the processing steps and enhances environmental compatibility, offering a clear advantage over other fluorine-free binders. Moreover, the work of Landi et al. reports a comparative analysis of chitosan, casein, gelatin, guar gum and

carboxymethyl cellulose in water-based electrolyte supercapacitor (1 M NaCl) [71]. Ageing tests performed on the obtained devices show a limited lifetime (the analysis is restricted to 1000 cycles) and during this period, a dramatic increase in ESR is observed, indicating the unsuitability of the proposed binders for water-based applications without further modification.

Among the water processable HPC, CMC, and LA133 binders, HPC can be synthesized from NC via etherification with propylene oxide in a NaOH/urea aqueous solution, followed by neutralization and purification steps involving water and acetone (Patent no. CN1205229C). This water-based, halogen-free synthesis pathway, although potentially energy-intensive and time-consuming, is advantageous for its moderate environmental impact and compatibility with circular bio-based sources. CMC is similarly derived from NC through carboxymethylation with monochloroacetic acid in ethyl alcohol media, involving alkali activation, etherification, and subsequent purification (Patent no. CN108473594B). While both HPC and CMC are biodegradable, the CMC synthesis process involves halogenated reagents and organic solvents, leading to a relatively higher production impact. In contrast, LA133 is a commercially available aqueous binder composed of polyacrylonitrile copolymers synthesized from petrochemical monomers such as acrylonitrile and acrylamide. Despite its utility in aqueous electrode formulations, LA133 exhibits a higher environmental impact due to its fossil-derived origin, non-biodegradability, and the presence of toxic monomers and has potential hazards as considered cancerogenic. With the available literature data, inference concerning the LCA of HPC with respect to fluorinated binder, PVDF [72], can be done by taking as equivalent case study the LCA data of Methylcellulose (MC) production, provided by EPD-Norway [73]. MC exhibits a significantly lower environmental impact than PVDF, with a global warming potential approximately ten times lower and an energy demand nearly seven times less. This contrast arises from MC's origin in renewable, biological sources such as wood pulp, in contrast to PVDF's fossil-based and fluorinated synthesis route. Additionally, MC is biodegradable and environmentally benign at end-of-life, whereas PVDF can release hazardous byproducts like hydrofluoric acid during degradation.

In this study, our objective is to explore the feasibility of utilizing HPC as a novel binder for large-scale electrochemical devices manufacturing. In this exploration, we aim to demonstrate particularly that HPC can substitute fluorinated binders, such as PVDF, in the manufacturing of capacitive electrodes for aqueous electrochemistry application. Currently, there is a lack of studies in the literature of the capabilities and advantages of HPC within the domains of batteries, supercapacitors, fuel cells, electrolyzers and related technologies, e.g., capacitive de-ionization. Herein, we mainly apply this material to produce SC electrodes in aqueous based slurry process and aqueous device by validating the efficacy of the salting out effect. Electrochemical stability at room temperature is addressed by means of standard characterization techniques such as cyclic voltammetry and galvanostatic cycling, and by means of ageing tests such as cyclability and the stressful floating tests. Thermal stability was addressed by thermal characterization techniques of electrode materials. Our findings reveal that HPC outperforms PVDF in terms of chemical stability in different aqueous environments, providing improved electrochemical performance. Moreover, specific surface area measurements and morphological characterizations revealed that HPC uniformly distributes the electrode material leading to promising perspectives in terms of different application scenarios.

2. Experimental

2.1. Electrode fabrication

Electrodes were fabricated through a standard procedure involving the deposition of a carbon-based slurry on a titanium (*Ti*) foil. The slurry composition was 85 wt% activated carbons (AC, YP-50F from Kuraray), 10 wt% of carbon black (CB, C65 from Imerys) and 5 wt% hydroxypropyl cellulose (HPC, Mw 370,000, from Sigma-Aldrich, CAS 9004-64-2) as binder in MilliQ water. To ensure a homogeneous mixture, the slurry was stirred for 6 h at 40 °C before being deposited onto a 20 μm thick *Ti* current collector (from Goodfellow) using doctor blade technique. The wet thickness was set to 150 μm. After the drying step at 60 °C, circular electrodes (d = 12 mm) were obtained by cutting the titanium foil with a pulsed nanoseconds fiber laser provided by Microla, emitting with a wavelength of 532 nm (power = 6.5 W and scan velocity of 25 mm s^{-1}. The final electrodes had a mass loading of 2.3 mg cm^{-2}. The same procedure was applied to obtain electrodes which have polyvinylidene fluoride (PVDF) as binder agent. However, in this instance, the slurry was composed of 85 wt% of AC and 10 wt% of PVDF (Mw 534,000, from Merck) and 5 wt% of carbon black (CB, C65 from Imerys) in dimethyl sulfoxide (DMSO, ≥99 %, from Merck, CAS 67–68-5). The two electrodes differ in CB and binder masses in terms of wt% due to the PVDF limitations. Indeed, to guarantee suitable active material adhesion, PVDF cannot be used below 10 wt%. For this reason, we changed the wt% of binder and CB, while keeping the relative amount of AC.

2.2. Physical-chemical characterizations

Electron microscopy characterization was carried out with a Field-Emission Scanning Electron Microscope (FESEM Supra 40, manufactured by Zeiss) equipped with a Si(Li) detector (Oxford Instruments) for Energy-Dispersive X-ray (EDX) spectroscopy.

Adhesion trials were conducted using a 180° peel configuration on a universal testing machine (FZ3-X500, Test Engineering) equipped with a load cell of 500 N. A commercial tape was attached onto the device and the free ends of both the tape and the titanium collector were clamped. The tests were performed at a constant speed of 5 mm min^{-1} until complete detachment occurred.

Specific Surface Area (SSA) measurements were carried out on both PVDF and HPC based electrodes to investigate the binder effect on the active material effective SSA. N_2 adsorption isotherms were performed at 77 K by means of ASAP2020 Plus, Micromeritics. The input weights for the SSA calculations were based on the mass of the active material only.

Thermogravimetric-coupled infrared absorption analyses (TGA-IR) were carried out in a thermogravimetric analyzer NETZSCH TG 209 F1 coupled by a transfer line heated at 230 °C with an infrared spectrometer Bruker TENSOR II equipped with an IR gas cell heated at 200 °C. The tests were performed by heating samples of about 3 mg in alumina pans from 30 °C to 800 °C with a rate of 20 K min^{-1}, under nitrogen flux of 20 mL min^{-1}. The FTIR analysis was collected in the absorbance mode in the range 4500–650 cm^{-1}. The first derivative of the weight profile (DTG) was calculated to better resolve the main thermal decomposition steps of the analysed materials with Netzsch Proteus Analysis software.

2.3. Electrochemical characterizations

Electrochemical tests were all performed in device configuration (2-electrodes), using a Swagelok T-cell exploiting 12 mm diameter electrodes. The separator was the glass fiber of grade D (GF/D) from Whatman, rinsed with 400 μL of electrolyte. The electrochemical properties of the fabricated electrodes were tested in acidic, neutral, and basic conditions. The electrolytes were prepared to perform experiments in 1 N conditions using H_2SO_4, Na_2SO_4, and KOH salts. The electrochemical measurements were performed with a *V*MP3 potentiostat provided by Bio-Logic.

Cyclic voltammetries (CV) were performed in the voltage window of [0, 0.8] *V* at increasing scan rates from 5.0 mV s^{-1} up to 1.0 V s^{-1} with quasi-logarithmic spacing. Voltammograms were recorded for 100 cycles at each scan rate. Electrochemical impedance spectroscopy (EIS) measurements were implemented at the open circuit voltage (OC*V*) by applying a sinusoidal signal with amplitude of V_p10 mV (V_p) and

frequency ranging from 1 MHz down to 10 mHz. Galvanostatic charge and discharge (GCD) measurements were carried out in the same voltage window of CV experiments, [0, 0.8] V. The current rate varied in the range from 0.1 A g^{-1} up to 10 A g^{-1}, recording at least 100 cycles per current rate. Two different ageing tests were performed to give further insight into the electrochemical stability of the electrode materials. Cycling stability (CS) and floating test (FT) were run in galvanostatic mode to address a comparative ageing between PVDF and HPC based electrodes. CS tests were performed at a fixed current rate of 1 A g^{-1} for 10,000 cycles. EISs were run every 500 cycles to monitor degradation at OCV. FTs were run by alternating 50 GCD cycles at 1 A g^{-1} with 20 h of constant voltage (CstV) periods at 0.8 V. Leakage currents (LCs) were recorded during the CstV periods. EIS measurements were performed at the beginning of the FT and after every CstV period to study the degradation mechanism at OCV.

The data analysis was performed using the following formulas:

- Capacity

$$Q_{c,d} = \int_{T_{c,d}} i(t)\, dt$$

- Energy and power

$$E_{c,d} = \int_{T_{c,d}} i(t)V(t)dt \quad P_d = \frac{E_d}{T_d}$$

- Coulombic and energy efficiencies

$$\eta_C = \frac{Q_d}{Q_c} \quad , \eta_E = \frac{E_d}{E_c}$$

- Capacitance

$$C_{device} = \frac{1}{2}\frac{Q_d^2}{E_d}$$

where $i(t)$ and $V(t)$ are, respectively, the current and the voltage in both potentiostatic and galvanostatic experiments. $T_{c,d}$ is the charging or discharging period considered for integrations. Specific quantities were calculated by dividing the computed quantities by the total amount of active material in the device, m_{tot}. Capacitance retentions were calculated with respect to the maximum rated capacitance within each experiment.

The Dunn's analysis [74] was implemented to study the eventual differences in terms of capacitance type-controlled mechanism differences between PVDF and HPC based devices in the different electrolytes. The method was implemented by analyzing the discharge peak currents by means of the following fitting function

$$i_p(v) = k_1 v + k_2 v^{0.5}$$

The fitting was carried out by weighting, w_i, the independent values, y_i, according to the variance weighting formula, $^1/_{y_i 2}$, to ensure a uniform fitting.

3. Results and discussion

The present work assumes that the salting-out effect of HPC in aqueous solutions may provide stability to EDLC electrodes operating in aqueous electrolytes. The 'salting-out effect' is defined as the separation of an organic phase from an aqueous phase by adding a salt [61]. Ternary phase solutions composed of solvent, water, salt and polymers can separate into salt-rich and polymer-rich phases. The phenomenon is based on both salt and polymer concentrations, and anion cation pair species, and it is mainly related to the shift in the cloud point of the dissolved polymer in temperature caused by the modulation of available solvent molecules for the polymer complexation. Based on this property of HPC, slurries were processed in de-ionized water (able to dissolve HPC) and then tested concentrated electrolytic solutions with the hypothesis that the polymer remained adsorbed in the electrode phase preserving its functional role. A similar concept was exploited in the work of Cheong et al., where the salting-out effect was exploited to confine the deposition of a water soluble polymer over a hydrophobic substrate [75].

3.1. Physical-chemical characterizations

Before electrochemical testing, the electrode was characterized by its physical properties. This includes the testing of its compatibility with water-based electrolyte and morphology investigation through electron microscopy method. Comparative FESEM images are reported in Fig. 1. Figures a) to d) are related to the surface morphology of HPC at different magnifications, while the ones from e) to h) are related to PVDF electrodes. In this figure it is possible to appreciate that at high magnification levels, the HPC electrode is not showing relevant macroporosities indicating a good cohesion and thus homogenous coating. There are no traces of HPC as AC and CB particles are clearly discernable. The inhomogeneous PVDF electrode, the poor interconnectivity between the AC particles, might imply a poor electrical interconnection between the AC particles and thus diffusions limitation through the electrode thickness. It is immediately clear that the HPC sample is more compact and homogeneous than the PVDF sample. From the point of view of the coverage, in the PVDF sample, voids represent 33 % of the area reported while in the case of the HPC sample, voids represent only 15 % of the area, as shown in Fig. 1d) and h).

The HPC electrode showed good mechanical properties, as reported in Fig. S2 in which there are reported pictures of the same coated titanium current collector under different bending radius conditions. The electrode stability in a saline solution was demonstrated by immersion in electrolytic solution for several days and we observed no material detachment as reported in the picture of Fig. S3. Moreover, 180° peeling tests were conducted to evaluate the adhesion strength between the coating and the titanium foil. A commercial adhesive tape was applied to each sample (HPC and PVDF), covering both an initial region of bare titanium and an area of coated titanium (Fig. 1i). From the graph force-displacement (Fig. 1j), both the samples initially exhibited a first tape elongation followed by a plateau at about 1.25 N. This force value corresponds to the tape adhesion to the bare titanium. Interestingly, a second step at approximately 2 N appears when the HPC coated part starts to be peeled (black curve). This area corresponds to the adhesive force of the HPC coated part, that is higher compared to the one of uncoated titanium, indicating a strong adhesion to the substrate. In contrast, this step is not observed for the PVDF-coated sample (red curve). In this case, the PVDF coating was completely removed during the test, remaining attached to the tape. The superior adhesion of HPC is confirmed by the visual images in Fig. 1k: the HPC layer resulted intact on the titanium substrate and no visual residuals were observed on the detached tape, whereas the PVDF was peeled off with the tape.

The effect of the electrode composition with respect to the AC surface area was investigated by means of isothermal surface area measurements. N_2 adsorption measurements were carried out at 77 K and the results are gathered in Table 1 and reported in Fig. 2. Additional information concerning the characterization of the bare YP-50F powder is reported in the Supporting Information, in Fig. S4 and Table S1. Samples were prepared by collecting coated slurries over titanium current collectors to observe the effects of electrode compositions and binder over the surface area properties. The data were normalized with respect to the actual AC mass in the two formulations, by neglecting then the not so influent contribution to the SSA from CB and binders.

Surface area measurements showed that the active material in the

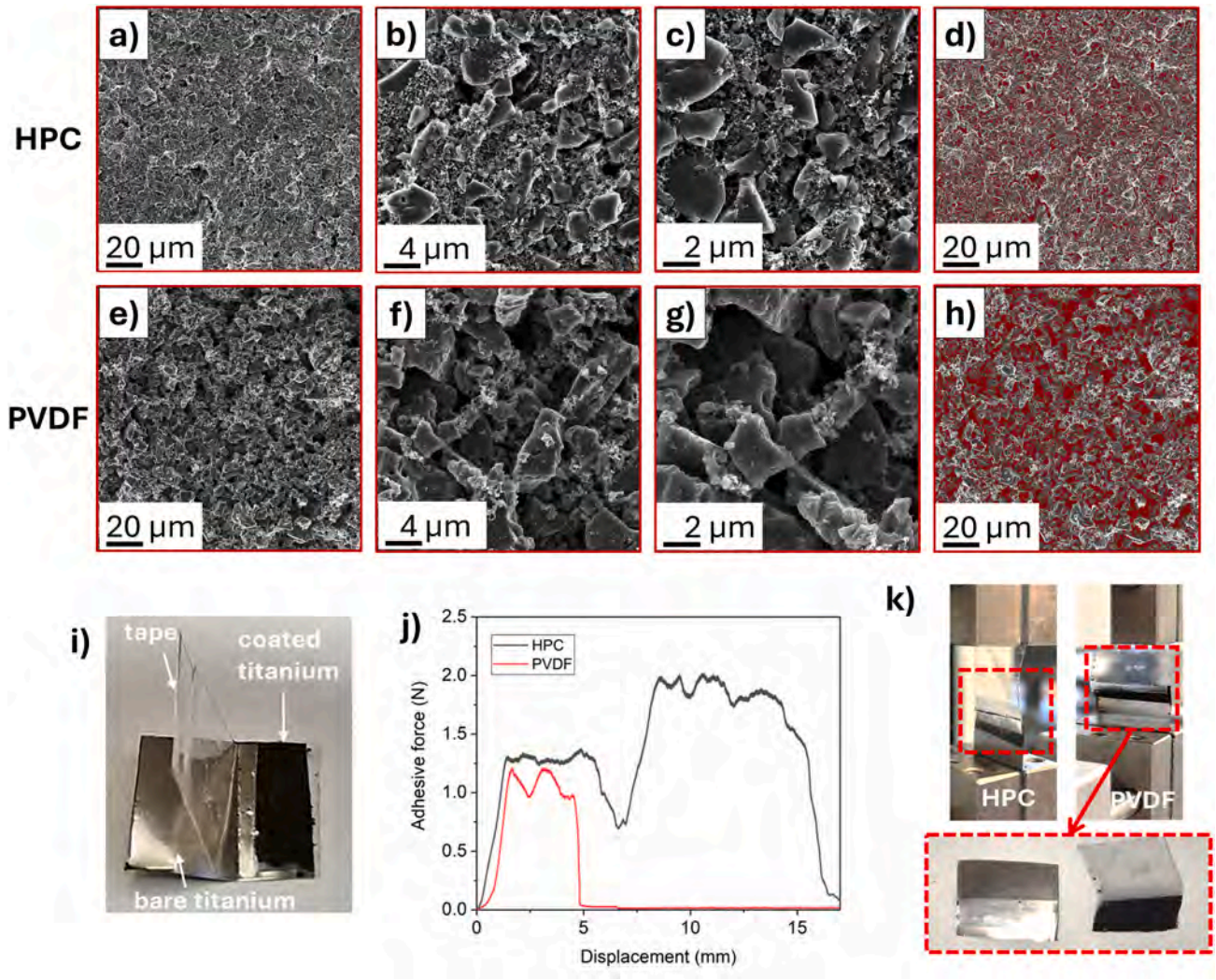

Fig. 1. Comparison between HPC (above, from a) to c)) and PVDF (below, from e) to g)) morphologies at different magnifications. In d) and h), the same figures of panels a) and e) but processed to highlight the macroporosities. In i) the sample for the adhesion test and in j) the resulting force-displacement curves. In k) optical images of the two samples subjected to peeling test. The areas where peeling occurs are highlighted in red. In the bottom, the PVDF sample after peeling test is reported.

Table 1
Surface parameters evaluated from N_2 adsorption measurements.

	Quantity	PVDF	HPC	Units	Notes
Isotherm	Single point Total Pore Volume	0.438	0.658	$cm^3\ g^{-1}$	@ 0.950 P/P_0
	Single point Surface Area	946.80	1431.0	$m^2\ g^{-1}$	@ 0.100 P/P_0
BET	Surface Area	943.82 ± 12.39	1436.1 ± 16.5	$m^2\ g^{-1}$	0.05–0.15 P/P_0
	Correlation Coefficient	0.9997	0.9997		
t-Plot	Micropore Volume	0.315	0.478	$cm^3\ g^{-1}$	0.38–0.44 nm
	Micropore Area	767.93	1174.7	$m^2\ g^{-1}$	
	External Surface Area	175.88	261.34	$m^2\ g^{-1}$	
NLDFT	Micropore Volume	0.094	0.146	$cm^3\ g^{-1}$	@ 2 nm
	Micropore Area	624.28	957.64	$m^2\ g^{-1}$	

formulation with HPC features a greater surface area, 1436.1 $m^2\ g^{-1}$, with respect to the PVDF one, 943.82 $m^2\ g^{-1}$, although normalized to the actual AC mass. Considering that the pristine AC powder showed, by means of the same measurement method, 1658 $m^2\ g^{-1}$, the electrode based on HPC has an SSA reduced by 13.4 %, while the PVDF based one features an impactful reduction of 42.9 %. This SSA reduction is mainly due to a loss in micropore area as can be seen from the cumulative surface area plot reported in Fig. 2b). Similar trends are found in the micropore volumes quantities with respect to the total pore volumes, considering that bare YP-50F rated 0.766 $cm^3\ g^{-1}$ with the single point quantity evaluated a 0.95 P/P_0, while 0.644 $cm^3\ g^{-1}$ with the t-plot method. These effects are caused by the pore blockage, which has been reported in literature where same killing factors have been rated [76–78]. According to the results reported in Table 1, the fraction of external surface area with respect to the BET one is similar for both slurries, being 18.2 % in the case of HCP sample and 18.6 % for the PVDF one. Although N_2 adsorption measurements are not accurate for pores >100 nm, the slightly more abundance in terms of external surface area for the PVDF is confirmed by the visible open spaces among the AC particles as appreciable from Fig. 1. Hence, our conclusion is that HPC can properly dissolve in the solvent and prevent pore blockage while keeping overall good mechanical properties of the electrodes. The pore

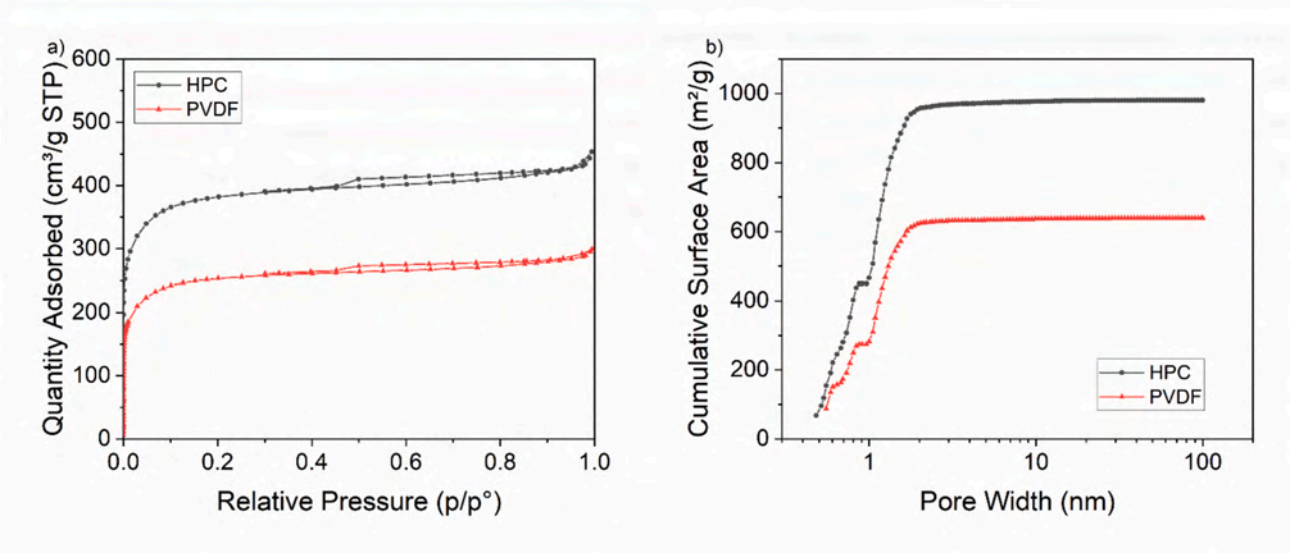

Fig. 2. In a) the isotherm recorded at 77 K showing the PVDF sample featuring higher surface area. In b) the cumulative surface area plot versus the pore size distribution.

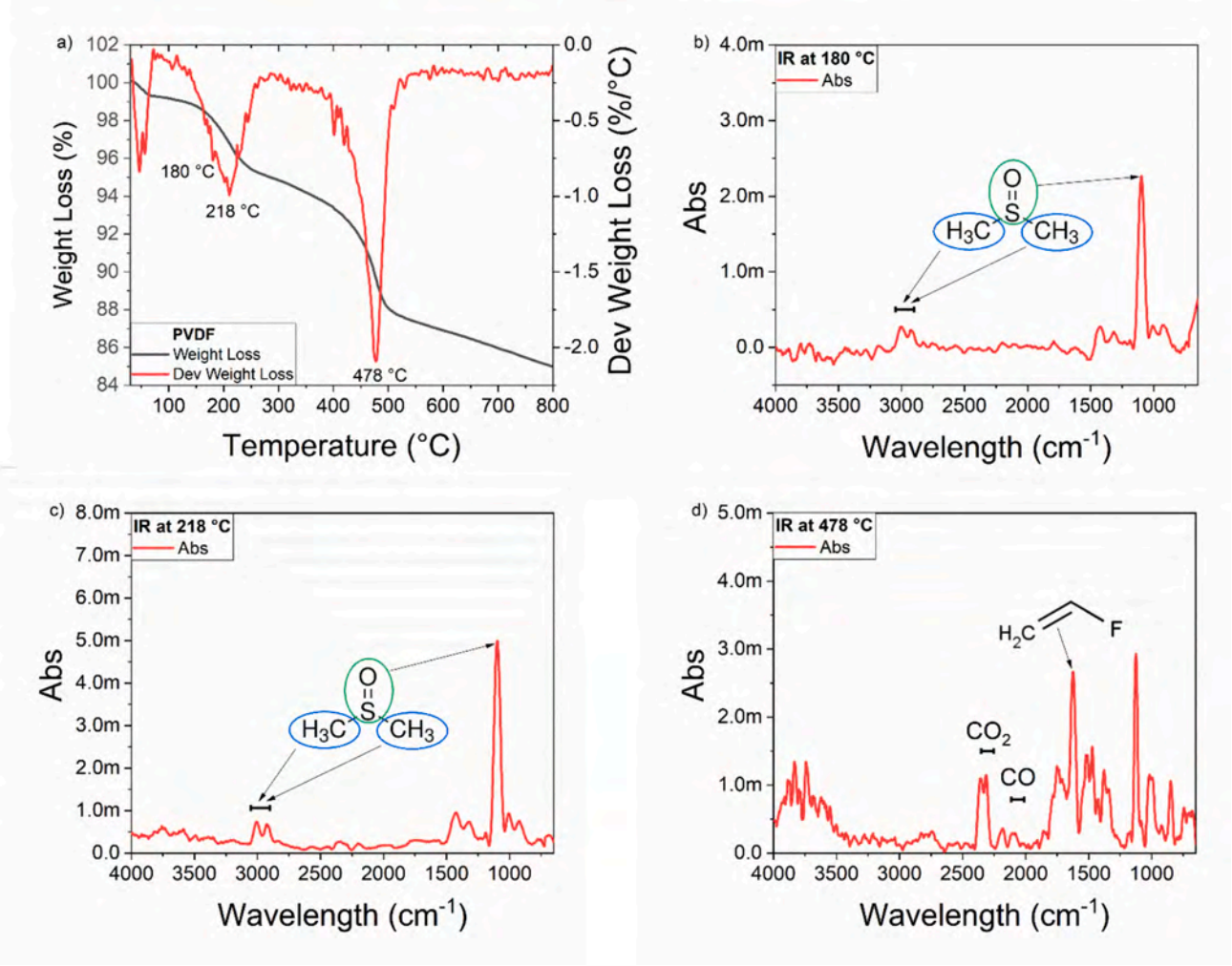

Fig. 3. In a) the TGA of the PVDF electrode material. b) Infrared spectra at 180 °C, c) Infrared spectra at 218 °C and d) Infrared spectra at 478 °C.

blockage hypothesis remains valid even when accounting for the measurement error in nitrogen adsorption reported by the porosimetry analyzer. Specifically, considering the maximum errors in SSA measurements (16.5 $m^2\ g^{-1}$ for the HPC sample and 12.39 $m^2\ g^{-1}$ for the PVDF one) the comparison continues to support this observation.

Electrodes were subjected to thermal analyses to study eventual thermal instabilities. PVDF is widely recognized for its exceptional chemical and thermal stability. However, under extreme conditions—such as elevated temperatures, exposure to radiation, or aggressive chemicals—it can decompose, releasing potentially hazardous by-products. The primary decomposition product is hydrofluoric acid, a highly toxic and corrosive substance formed through the elimination of fluorinated groups. Additionally, degradation can generate volatile fluorinated compounds, such as vinylidene fluoride (VDF) monomer, tetrafluoroethylene, and smaller fluorocarbons like fluoromethane and difluoromethane. In oxidative conditions, gases like carbon dioxide and carbon monoxide may also be released. At higher temperatures or prolonged exposure, carbonaceous residues can remain as solid by-products. By contrast, while HPC also undergoes thermal degradation above 250 °C [79], it does not contain or release halogenated species. As shown in the thermogravimetric analysis of pure HPC, the primary degradation stage occurs between 220 °C and 360 °C, with mass loss attributed to depolymerization and breakdown of the cellulose ether backbone. The emitted products, such as acetone and propanal, although volatile and flammable, are less acutely toxic and non-corrosive. Therefore, from a thermal safety standpoint, HPC poses significantly lower hazard than PVDF, especially in scenarios involving fire or high-temperature malfunction.

Thermogravimetric analysis revealed a decomposition peak at 50 °C (Fig. 3a), primarily attributed to the evaporation of water absorbed by PVDF during electrode exposure to atmosphere. Also, the presence of residual solvents such as DMSO (Fig. 3b) is easily identifiable as the primary product in the decomposition bands with maximum intensities at 180 °C and 210 °C, with characteristic IR bands between 3000 and 2900 cm^{-1}, corresponding to the symmetric and asymmetric stretching of the CH_3 groups, and the stretching of the S═O bond around 1100 cm^{-1}, according to the NIST database [80] accessed January 30, 2025, (Fig. 3c). Further degradation occurs at 480 °C (Fig. 3d), where PVDF decomposition products become evident. These include hydrofluoric acid (HF) [81], a highly toxic and corrosive substance formed through the elimination of fluorinated groups. Additionally, volatile fluorinated compounds such as vinylidene fluoride with a C═C monomer stretching around 1630 cm^{-1}, according to the NIST database [82], tetrafluoroethylene (TFE) not visible at IR, and smaller fluorocarbons like fluoromethane and difluoromethane are released. Under oxidative conditions, or in the presence of oxidized heteroatoms (e.g. DMSO presence) gases like carbon dioxide (CO_2) (band around 2275 cm^{-1}) and carbon monoxide (CO) the two bands between 2000 cm^{-1} and 2100 cm^{-1} are also emitted, with carbonaceous residues remaining as solid by-products at higher temperatures or after prolonged exposure. Given the toxicity and environmental impact of these by-products, particularly HF, an effective mitigation strategy involves reconsidering the use of PVDF in applications where thermal or chemical degradation could pose risks.

Thermal analyses were also run on HPC based electrode samples. HPC exhibits continuous weight loss, attributed to the release of hydration water (Fig. 4a). At around 350 °C, a significant degradation peak is observed, corresponding to the loss of the hydroxypropyl functional group. This decomposition is confirmed by IR spectroscopy, which identifies two distinct products resulting from the reorganization of the binder: propanal and acetone. Propanal is characterized by a C═O stretching band at 1750 cm^{-1}, alongside CH stretching bands ranging from 3100 cm^{-1} to 2600 cm^{-1}, which are indicative of the aldehydic group and the ethyl group. Acetone displays a C═O stretching band at the same wavenumber, 1750 cm^{-1}, with CH stretching bands in the range of 3100 cm^{-1} to 2800 cm^{-1}, corresponding to methyl groups. The IR spectra of these compounds in the gas phase are consistent with data from the NIST Chemistry WebBook with references to the propanal [83] and acetone [84].

These spectral features confirm the decomposition pathway of HPC at elevated temperatures, as the C═O stretching bands are distinct, and the CH stretching regions for propanal and acetone, although partially overlapping, show unique patterns that allow clear identification of both compounds.

3.2. Electrochemical characterizations

A preliminary study of each assembled device was performed by using cyclic voltammetry (CV), galvanostatic charge-discharge (GCD), and electrochemical impedance spectroscopy (EIS). The results are reported in Fig. 5. CV is considered a suitable technique to explore the capacitive behavior of any electrode material and in Fig. 5a) it is possible to notice the standard quasi-rectangular shape of the CVs for all the assembled HPC-based devices with different electrolytes. Under the same scanning conditions, voltammograms with larger current suggest a higher specific capacitance. Specifically, our data show that $KOH > H_2SO_4 > Na_2SO_4$ in this respect. Similar trends were observed for PVDF devices. In Fig. S5 we report the EIS spectrums of both HPC and

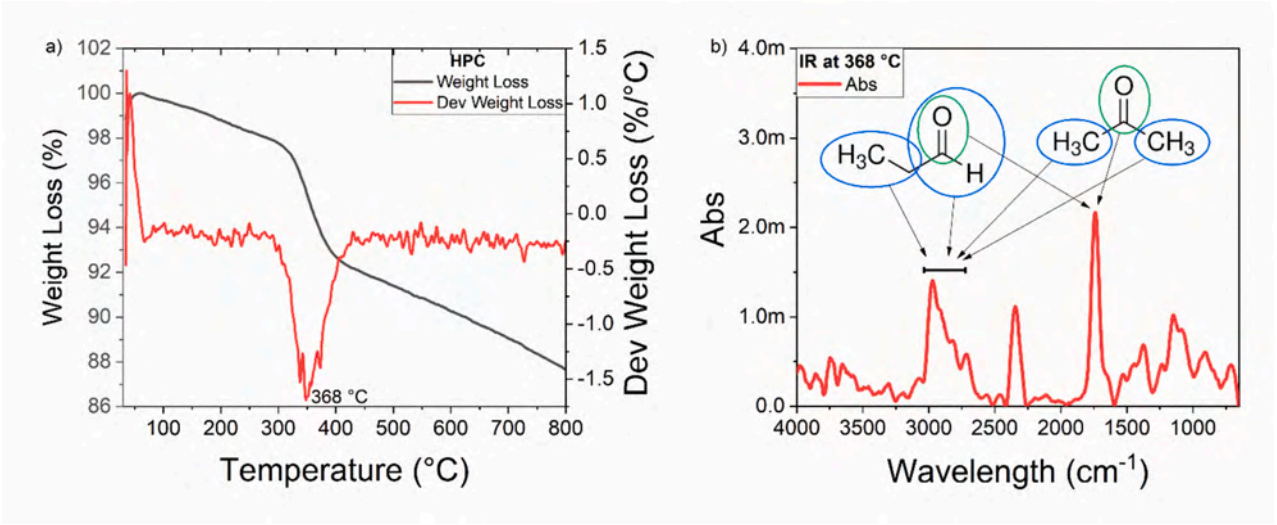

Fig. 4. In a) the TGA of HPC electrode material and in b) the Infrared spectra at 368 °C.

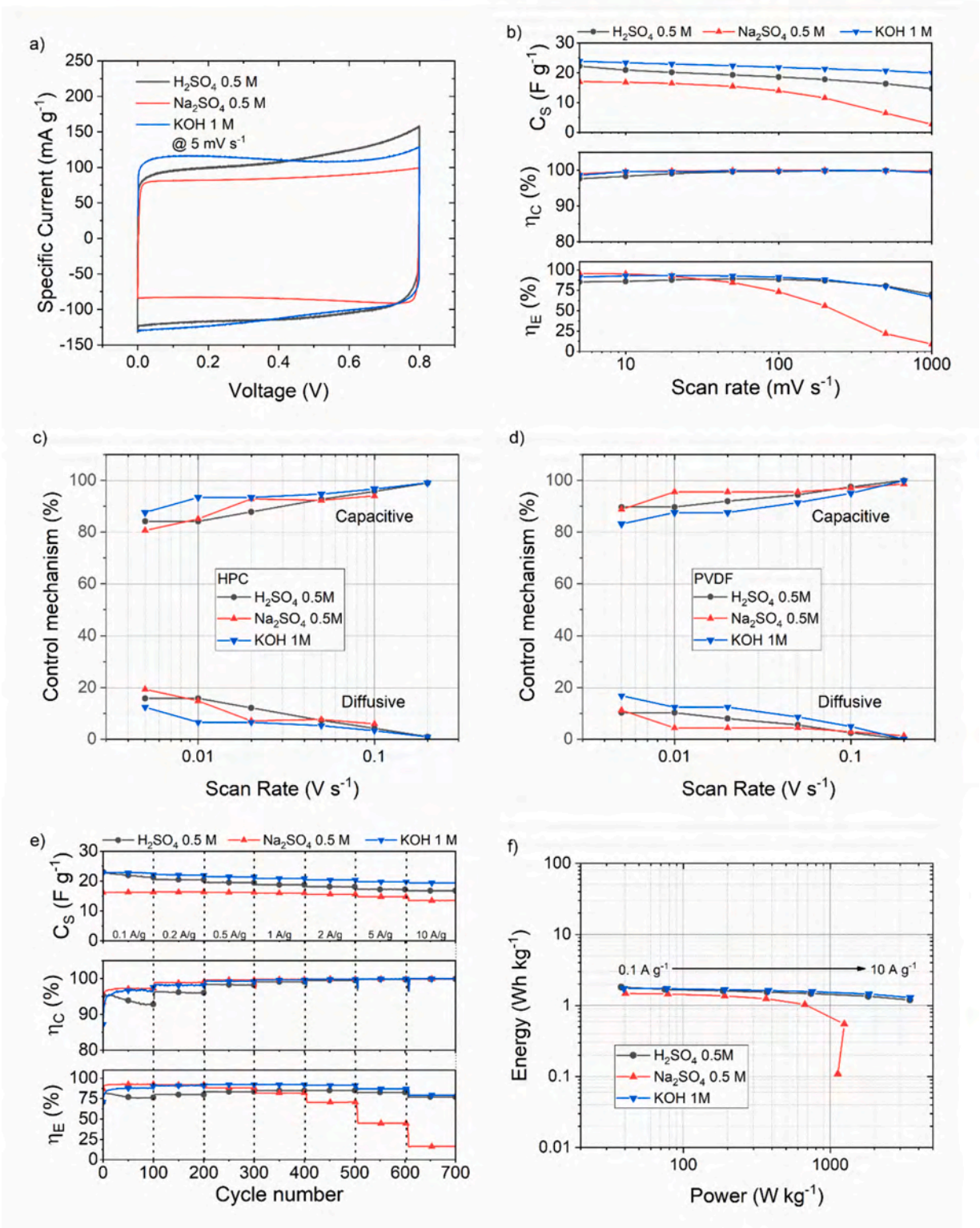

Fig. 5. In a) the i-v characteristics of the three devices assembled with HPC electrodes. In b) specific capacitance, coulomb and energy efficiencies reported vs. the scan rate variation. Comparison between HPC, in c), and PVDF, in d), based devices capacitive contributions according to the Dunn analyses. In e), the variations of specific capacitance, coulomb and energy efficiencies vs. cycle number resulting out of the GCD test performed at {0.1, 0.2, 0.5, 1.0, 2.0, 5.0, 10.0} A g^{-1}. In f), the Ragone plot resulting from the GCD test.

PVDF based devices. According to the obtained EIS result, the acidic system features the lowest series resistance value and almost no electrodes parasitic behavior while neutral and basic device show a slight parasitic behavior at high frequencies [85]. In the case of PVDF devices, the larger semicircle diameter could be addressed to an increased parasitic behavior due to a more inhomogeneous electrode phase, as demonstrated by the FESEM images of Fig. 1. However, based on the discussions reported in the work of Köps et al., regardless of the high

frequency behavior, the device features similar resistive behavior in the low frequency region implying similar internal resistance [86]. Evaluations of the equivalent series and internal resistances (IR) are reported in Table S2. These results suggest that HPC devices are more resistive, however, since EIS measurements were done at OCV, it is possible to state (based on the rate capability test results reported in Fig. S6) that presumably the IR value of PVDF devices slightly overcome the one of HPC devices upon polarization.

It is interesting to compare the specific capacitances achieved when employing HPC as binder versus those obtained with PVDF. Capacitance values were calculated from the 50th cycle of the CV performed at 5 mV s^{-1}. The summarized results reported in Table 2 demonstrate how the cellulose binder leads to higher specific capacitances for each examined electrolyte system. This is likely due to PVDF blocking the porosity of the active material [87,88]. Further proof supporting this claim comes from the reported SSA measurements out of which a SSA reduction was observed for PVDF based electrodes.

In Fig. 5b) we report the scan rate analyses results of the sole HPC based devices. As the scan rate increases, the specific capacitance diminishes, yet the trends remain largely consistent. In fact, the lowest C_S can be associated to the neutral electrolyte, meanwhile the acidic and the basic one exhibit similar capacitance retentions. Regarding energy efficiency, devices utilizing *KOH* and Na_2SO_4 as electrolytes outperform the H_2SO_4-based device at low scan rates. However, this behavior changes at higher scan rates. The trend might indicate reduced stability of the acidic device because, at low scan rates, the characteristic time constant could match the degradation rate. This possibility is supported by the low coulombic efficiency. This behavior is present in both cases (HPC and P*V*DF), which means that it is not a binder compatibility issue. A possible explanation can be the corrosion of the titanium current collector (see Fig. S7 for further details), as reported in the work of Krika et al. [89]

The observed trend aligns with expectations for a capacitive double-layer system, moving towards more resistive behavior, namely a lower energy efficiency, as the scan rate is increased from 5.0 mV s^{-1} to 1.0 V s^{-1}. In Fig. S6, we report a comparative analysis of the rate capability of the different devices coming from the CV measurements in which it is evident that, apart from the neutral case, HPC based devices outperform PVDF based ones.

Further insight was given to the CV measurements to discriminate the type of capacitive contributions due to the different electrodes. As shown in the graphs in Fig. 5c) and d), an analysis was performed by applying Dunn's model to the cells at different pHs. The selected scan rates were {5, 10, 20, 50, 100, 200} mV s^{-1}. The last scan rates were neglected in some cases due to possible instrumental issues. Experimental evidence suggests a slightly elevated diffusive contribution percentage at low scan rates. According to the literature, activated carbon has a pseudocapacitive contribution from 5 to 10 % [90]. This kind of phenomenon together with ions drift-diffusion limitations in pore structures, are the main contributors to diffusion controlled capacitive storage mechanism in AC-based electrodes. Provided that the activated carbon is the same for both electrode types, it is possible to conclude that the charge storage mechanism is characterized by an important contribution of mass limitation. This proves the similar rate capabilities observed in the CV experiments. Details concerning the fitting results are reported in Table S3 and Fig. S8. The fitting was carried out by weighting, w_i, the y_i values according to the variance weighting formula, $^1/_{y_i}{}^2$, to ensure a uniform fitting.

Table 2
summary of the calculated specific capacitances of the different assembled devices obtained from the CV measurement recorded at 5 mV s^{-1}.

	H_2SO_4	Na_2SO_4	*KOH*
HPC	22.21 F g^{-1}	17.03 F g^{-1}	23.86 F g^{-1}
PVDF	19.18 F g^{-1}	13.91 F g^{-1}	16.70 F g^{-1}

GCD measurements were run to determine the power capabilities of the three devices. Devices were cycled 100 cycles per current rate at {0.1, 0.2, 0.5, 1.0, 2.0, 5.0, 10.0} A g^{-1}. The results of these measurements are reported in Fig. 5e). The H_2SO_4 device rated low coulombic and energy efficiencies at low rates as in the CV rate capability test. Galvanostatic data suggests that the maximum current rates are: 2 A g^{-1} for Na_2SO_4, while both *KOH* and H_2SO_4 can operate quite well at 10 A g^{-1}. Energy efficiency is consistent with the internal resistance trends reported in Table S2 starting from 1.0 A g^{-1} where the acidic device is not affected by degradation due to the relatively high rate. In Fig. 5f) it is reported the Ragone plot derived from the GCD measurements. This result further confirms the rate capability results reported for both CV and GCD. Despite the low efficient behavior at low characterization rates, the device operating in acidic electrolyte can operate at 1.0 kW kg^{-1} while delivering an energy density above 1.0 Wh kg^{-1}. These results suggest that overall, the presented systems assembled with HPC binder-based electrodes are sufficiently stable in the diverse electrolytic systems, in particular Na_2SO_4 and *KOH* electrolytes. A possible explanation for the increased rate capabilities of HPC in acidic media can be that the HPC device operating in acidic environment shows no parasitic features with respect to Na_2SO_4 and *KOH* devices as depicted in Fig. S4. Similar results can be found in literature [34]. This explanation is further supported by the difference found between the EIS results between HPC and PVDF devices in acidic environment as can be evinced from Fig. S5.

Long cycle stability tests were performed after the initial analysis. 1.0 A g^{-1} was selected as common current rate density for the galvanostatic cyclability test for 10,000 cycles. The results are reported in Fig. 7. The stability of devices is underlined by capacitance retention plots $\left(C/C_{max}\,\%\right)$ reported in Fig. 7a) and b) for HPC and PVDF devices, respectively. After the entire experiment, devices based on *KOH* and Na_2SO_4 experience an almost 8 % decrease in capacitance, whereas the H_2SO_4 one experiences just a 1 % decrease. However, by examining the plot of Fig. 7a), it is interesting to notice the initial decrease in C_S and successive increase during the middle cycles in the case of the acid system. This behavior can be linked to an overall net conditioning of the electrodes, namely an enhanced wettability of carbon while cycling, and its possible activation [91]. To check the state of the devices, we performed an impedance spectroscopy every 500 charge-discharge cycles. The changes observed in the EIS data are reported in Fig. S9a,c,e) in the case of HPC based devices, and in Fig. S9b,d,f) for PVDF based devices. Cases of Fig. S9a) and b) regard the acidic systems. It is possible to appreciate that in both cases an increase in the parasitic electrode behavior, more pronounced in the HPC case. The enlargement of the semicircle at high frequencies and the slope's variation indicates a degradation in device performance over cycling, as evidenced also by the low coulombic efficiency especially during the first cycles. This behavior can be explained by considering the titanium collector corrosion in acidic environments and consequent slight loss of electrical contact between the current collector and the active material phases. Potential alternatives for the acidic environment can be paper-based expanded graphite (EG), glassy carbon or porous graphene [79,83]. Fig. 6 shows two cyclic voltammetries performed in batch acidic solution with gold and glassy carbon as current collectors. From these three electrode characterizations can be noted almost rectangular standard CV profile. Under the same scanning conditions, the voltammogram with higher current provides a higher specific capacity due to the different mass loading that was not tuned during the preparation phase. The aim of this test is to prove that the HPC binder serves as adherent material for different current collectors. However, in view of a potentially scalable application, both glassy carbon and gold are less preferred due to the high costs, different mechanical properties, and viability as foil current collector format.

In Fig. S9c) and d) are reported the cases related to the neutral environment. In this case, the PVDF device showed remarkable stability

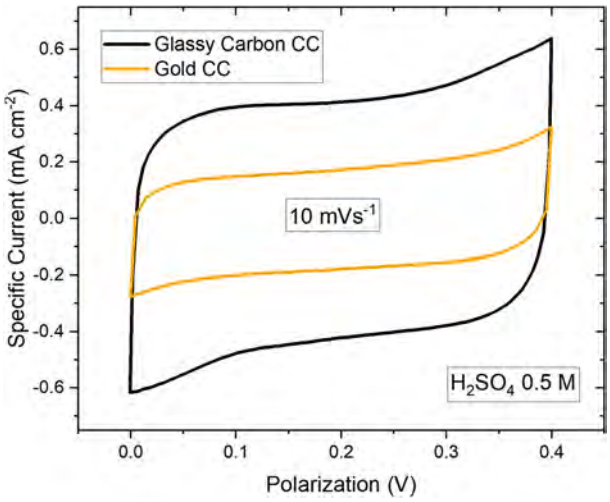

Fig. 6. Cyclic voltammetry of electrodes prepared with the HPC slurry on glassy carbon and gold current collectors. The tests were conducted in acid environment, H_2SO_4 0.5 M, to test the stability of the HPC-based active material on different current collector substrates. (For interpretation of the references to color in this figure legend, the reader is referred to the web version of this article.)

over cycling whereas the HPC device showed a slight increase in resistive behavior. A slight variation of the internal resistance over cycling was observed for the neutral system, and this is reflected in the slightly lower, but stable, energy efficiency recorded with respect to the neutral case in the PVDF system. While the exact cause remains unclear, the following discussion explores possible explanations. During the more stressful floating test, the neutral system is stable in both HPC and PVDF cases, with no substantial internal resistance variation [92]. The reaction between PVDF binder and KOH electrolyte solution is evident in Fig. S9e) and f) where the EIS data worsen over cycling and both data about energy efficiency and capacitance retention indicate a non-stable device, as reported in Fig. 7b). On the contrary, in acidic and neutral conditions, both binders demonstrate comparable performance in terms of efficiency and capacitance retention.

To conclude, the above-mentioned HPC stability was further validated through float tests, in which the device is maintained at 0.8 V for 20 h. After this period, an EIS is performed to evaluate the impedance variations and 50 GCD cycles are run at 1.0 A g^{-1} to evaluate the device capacitance. This process is repeated several times for each configuration. FT results are summarized in Fig. 8 and compared between HPC and PVDF devices. Data show capacitance retention above 90 % and high efficiencies throughout the test for HPC-based devices, as depicted in Fig. 8a). Concerning PVDF-based devices, capacitance retention is still above 90 % in the case of neutral and acidic systems, energy and coulomb efficiency are comparable with HPC-based devices, as reported in Fig. 8b). However, the basic system showed a much more stressful degradation with respect to the CS test. The present result, as discussed also for the cyclability test results, is derived from considering the calculated values at the GCD rate of 1.0 A g^{-1}. This current rate is sufficiently fast not to let the degradation phenomena being observed in terms of coulomb and energy efficiencies calculations. Based on results from this accelerated ageing test, we conclude that the active material, comprising the binder, is not substantially degraded since the capacitance retention remained consistently high. Thanks to the leakage currents recorded during the floating periods, however, we concluded that the only cell part degrading in the acidic environment is the titanium current collector. Further evidence of both stability and instability can be found in Fig. 8 where EIS spectrums (recorded at OCV) are reported per floating cycle, first (light color) and last (bulk color). Degradation is definitively evident in the case of the PVDF device in basic media. At the end of the floating test the cell became insanely resistive. In the case of the neutral systems, although slight variations in the real part at high frequencies, both devices showed no substantial internal resistance variation. Slight variations in the resistance are observed in the acidic system due to the current collector degradation. This explanation is provided since, concerning the leakage current, this is almost ten times higher in acidic conditions; it gets worse with each cycle. This behavior is evident in both HPC and PVDF cases (Fig. S10). Except for the alkaline case where the HPC performs better, data also reveal similar leakage currents between PVDF and HPC based devices. Values remained below a limiting value of 1 mA g^{-1}, except in cases where current collector corrosion is favored and in the case of PVDF dehydrofluorination. A comparison of the most relevant figures of merit are available in the Supporting Information (Table S4, Fig. S11).

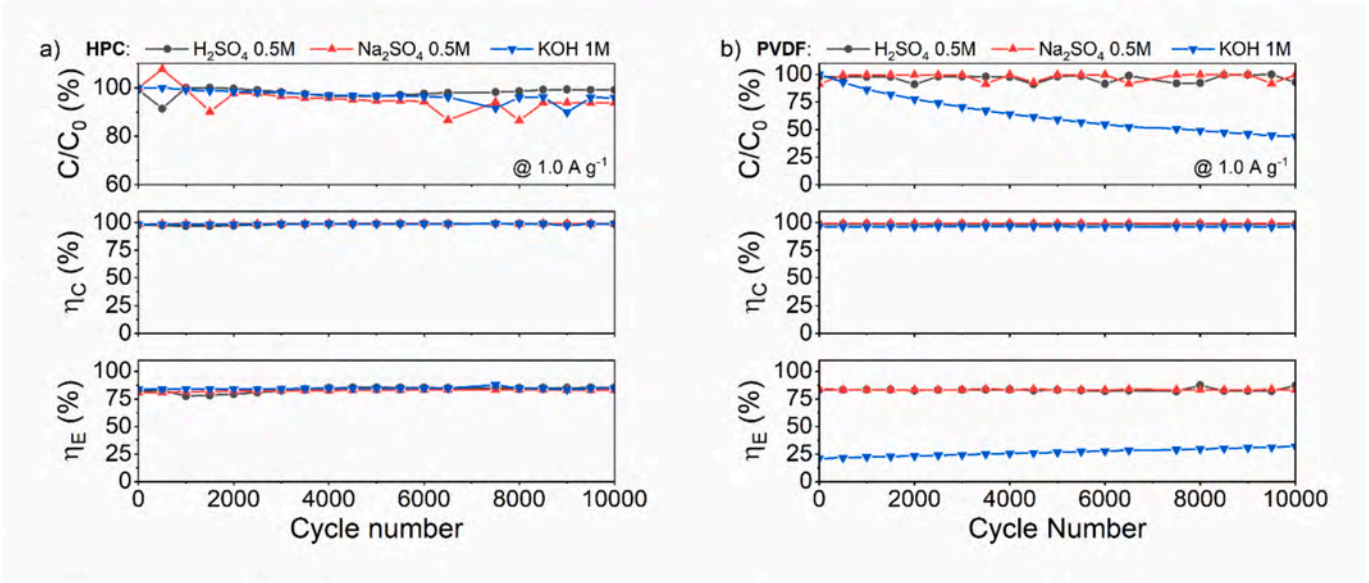

Fig. 7. Cycling stability GCD test of 10,000 cycles at 1.0 A g^{-1}. In a) and b) the capacitance retention, coulomb and energy efficiencies vs. cycle number, derived from the galvanostatic cycling at 1.0 A g^{-1} for HPC and PVDF devices, respectively.

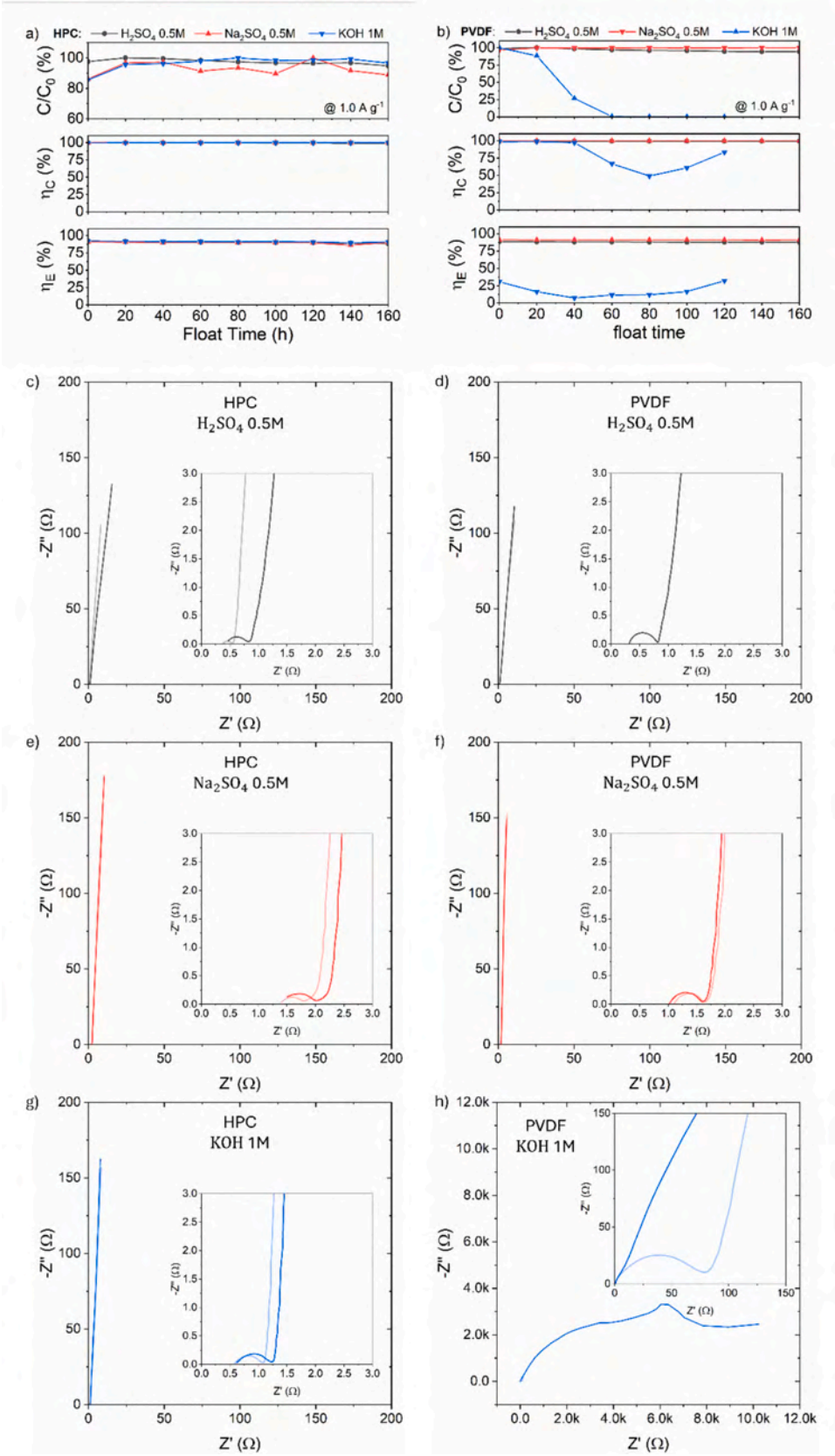

Fig. 8. Floating Test results. In a) and b) the capacitance retention, coulomb and energy efficiencies vs. the floating time, derived from the galvanostatic cycling at 1.0 A g^{-1} for HPC and PVDF devices, respectively. In c,e,g) and d,f,h) the first and last EIS measurement recorded during the FT for HPC and PVDF devices, respectively.

4. Conclusion

The present work demonstrates that hydroxypropyl cellulose (HPC) is a viable, sustainable alternative to fluorinated binders like PVDF for supercapacitor electrodes in aqueous electrolytes. HPC enabled water-based processing and showed strong performance across acidic, neutral, and basic media, respectively 1 N H_2SO_4, Na_2SO_4, and KOH. Compared to PVDF, HPC-based electrodes exhibited improved structural uniformity, chemical and thermal stability, adhesivity and enhanced electrochemical performance, particularly in basic environments where PVDF degrades. These results highlight HPC's potential as a versatile binder for electrochemical energy storage devices. In terms of device performance, the HPC devices showed greater capacitance with respect to PVDF devices. HPC devices scored almost 22.21 F g^{-1} in acidic environment, 17.03 F g^{-1} in neutral media, and 23.86 F g^{-1} in basic electrolyte. Both after GCD 10000 cycles and 160 h of floating test, HPC devices showed a capacitance retention >90 %, especially in the case of basic media in which the PVDF device turned to be unstable. Perspectives on the development of more reliable devices can be the study of these systems with much stabler current collectors to improve the overall performance especially in acidic media. Further, investigation of HPC crosslinking for high mass loading material is envisioned soon, as well as testing the electrode formulations in organic electrolytes.

CRediT authorship contribution statement

Simone Martellone: Writing – review & editing, Writing – original draft, Visualization, Methodology, Investigation, Formal analysis, Data curation. **Davide Molino:** Writing – review & editing, Writing – original draft, Visualization, Methodology, Investigation, Formal analysis, Data curation. **Davide Arcoraci:** Writing – review & editing, Writing – original draft, Visualization, Methodology, Investigation, Formal analysis, Data curation. **Giorgio Mogli:** Writing – review & editing, Writing – original draft, Visualization, Methodology, Investigation, Formal analysis, Data curation, Conceptualization. **Mara Serrapede:** Writing – review & editing, Visualization, Methodology, Investigation, Formal analysis, Data curation. **Giuseppe Ferraro:** Writing – review & editing, Writing – original draft, Visualization, Methodology, Investigation, Formal analysis, Data curation. **Alessandro Pedico:** Writing – review & editing, Writing – original draft, Visualization, Methodology, Investigation, Formal analysis. **Sergio Bocchini:** Writing – review & editing, Writing – original draft, Visualization, Methodology, Investigation, Formal analysis, Data curation. **Pietro Zaccagnini:** Writing – review & editing, Writing – original draft, Validation, Supervision, Methodology, Investigation, Formal analysis, Data curation, Conceptualization. **Andrea Lamberti:** Writing – review & editing, Visualization, Validation, Supervision, Funding acquisition, Conceptualization.

Declaration of competing interest

The authors declare the following financial interests/personal relationships which may be considered as potential competing interests:

Andrea Lamberti reports financial support was provided by European Research Council. Andrea Lamberti reports financial support was provided by Government of Italy Ministry of Research. Andrea Lamberti reports financial support was provided by Government of Italy Ministry of Energy Transition. If there are other authors, they declare that they have no known competing financial interests or personal relationships that could have appeared to influence the work reported in this paper.

Acknowledgements

The authors wish to acknowledge Dr. Paulo Luís from the CICenergyGUNE for the useful discussions on HPC possible crosslinking reaction during the ISEECAP conference held in 2024 in Vitoria-Gasteiz.

This work was partially funded under the National Recovery and Resilience Plan (NRRP), Mission 4 "Education and Research"-Component 2 "From research to business"- Investment 3.1 "Fund for the realization of an integrated system of research and innovation infrastructures"-Call for tender No. N. 3264 of 28/12/2021 of Italian Ministry of Research funded by the European Union-NextGenerationEU-Project code: IR0000027, Concession Decree No. 128 of 21/06/2022 adopted by the Italian Ministry of Research, CUP: B33C22000710006, Project title: iENTRANCE.

This research work has been supported also by the "Progetto Orangees - ORgANics for Green Electrochemical Energy Storage – codice CSEAA_00010" funded by the Italian Government through the MITE (Ministero della Transizione Ecologica) call 2022 "Bandi di gara di tipo A".

This result is part of a project that has received funding from the European Research Council (ERC) under the European Union's ERC Starting Grant agreement "CO2CAP" No. 949916. This manuscript reflects only the authors' views and opinions, neither the European Union nor the European Commission can be considered responsible for them.

Appendix A. Supplementary data

Supplementary data to this article can be found online at https://doi.org/10.1016/j.est.2025.117532.

Data availability

Data will be made available on request.

References

[1] G. Hernández, R. Mogensen, R. Younesi, J. Mindemark, Fluorine-free electrolytes for Lithium and sodium batteries, Batter. Supercaps. 5 (2022) e202100373, https://doi.org/10.1002/batt.202100373.

[2] F.A. Kreth, L. Köps, C. Leibing, S.D. Magar, M. Hermesdorf, K. Schutjajew, C. Neumann, D. Leistenschneider, A. Turchanin, M. Oschatz, J. Luis, G. Urbano, A. Balducci, Enabling fluorine-free Lithium-ion capacitors and Lithium-ion batteries for high-temperature applications by the implementation of Lithium Bis (oxalato) borate and ethyl isopropyl sulfone as electrolyte, Adv. Energy Mater. 14 (2024) 2303909, https://doi.org/10.1002/aenm.202303909.

[3] N.T.M. Baltes, J. Heumann, P.M. Rabenecker, J. Tübke, Vinyl acetate-ethylene as a potential alternative to fluorine free binders in supercapacitors, Chem. Eng. J. 476 (2023) 146517, https://doi.org/10.1016/j.cej.2023.146517.

[4] B. Babu, P. Simon, A. Balducci, Fast charging materials for high power applications, Adv. Energy Mater. 10 (2020) 2001128, https://doi.org/10.1002/aenm.202001128.

[5] S. Dong, N. Lv, Y. Wu, G. Zhu, X. Dong, Lithium-ion and sodium-ion hybrid capacitors: From insertion-type materials design to devices construction, Adv. Funct. Mater. 31 (2021) 2100455, https://doi.org/10.1002/adfm.202100455.

[6] H. Tang, J. Yao, Y. Zhu, Recent developments and future prospects for zinc-ion hybrid capacitors: A review, Adv. Energy Mater. 11 (2021) 2003994, https://doi.org/10.1002/aenm.202003994.

[7] Y. Wu, Y. Sun, Y. Tong, X. Liu, J. Zheng, D. Han, H. Li, L. Niu, Recent advances in potassium-ion hybrid capacitors: Electrode materials, storage mechanisms and performance evaluation, Energy Storage Mater. 41 (2021) 108–132, https://doi.org/10.1016/j.ensm.2021.05.045.

[8] X. Liu, Y. Sun, Y. Tong, X. Wang, J. Zheng, Y. Wu, H. Li, L. Niu, Y. Hou, Exploration in materials, electrolytes and performance towards metal ion (Li, Na, K, Zn and mg)-based hybrid capacitors: A review, Nano Energy 86 (2021) 106070, https://doi.org/10.1016/j.nanoen.2021.106070.

[9] P. Srimuk, F. Kaasik, A. Tolosa, S. Fleischmann, J. Nicolas, M.C. Tekeli, M. Aslan, MXene as a novel intercalation-type pseudocapacitive cathode and anode for capacitive deionization, J. Mater. Chem. A 4 (2016) 18265–18271, https://doi.org/10.1039/c6ta07833h.

[10] M. Thomas, C. Cannilla, A. Brigandì, I. Nicotera, F. Lufrano, Nanoarchitectonics of high-performance supercapacitors based on mesoporous carbon and MnO2 electrodes using Aquivion electrolyte membrane, J. Alloys Compd. 960 (2023) 170719, https://doi.org/10.1016/j.jallcom.2023.170719.

[11] R. Demir-cakan, M. Morcrette, J. Leriche, J. Tarascon, An aqueous electrolyte rechargeable Li-ion/ polysulfide battery, J. Mater. Chem. A 2 (2014) 9025–9029, https://doi.org/10.1039/c4ta01308e.

[12] R. Demir-cakan, M. Morcrette, J. Tarascon, Use of ion-selective polymer membranes for an polysulphide battery †, J. Mater. Chem. A Mater. Energy Sustain. 3 (2014) 2869–2875, https://doi.org/10.1039/C4TA05756B.

[13] A.J. Paleo, P. Staiti, A.M. Rocha, G. Squadrito, F. Lufrano, Lifetime assessment of solid-state hybrid supercapacitors based on cotton fabric electrodes, J. Power Sources 434 (2019) 226735, https://doi.org/10.1016/j.jpowsour.2019.226735.

[14] R. Lohmann, I.T. Cousins, J.C. Dewitt, J. Glüge, G. Goldenman, D. Herzke, A. B. Lindstrom, M.F. Miller, C.A. Ng, S. Patton, M. Scheringer, X. Trier, Z. Wang, Are fluoropolymers really of low concern for human and environmental health and separate from other PFAS? Environ. Sci. Technol. 54 (2020) 12820–12828, https://doi.org/10.1021/acs.est.0c03244.
[15] B.J. Henry, J.P. Carlin, J.A. Hammerschmidt, R.C. Buck, L.W. Buxton, A critical review of the application of polymer of low concern and regulatory criteria to fluoropolymers, Ntegrated Environ. Assess. Manag. 14 (2018) 316–334, https://doi.org/10.1002/ieam.4035.
[16] D. Savoca, A. Pace, Bioaccumulation, biodistribution, toxicology and biomonitoring of organofluorine compounds in aquatic organisms, Int. J. Mol. Sci. 22 (2021) 6276, https://doi.org/10.3390/ijms22126276.
[17] T.C. Nirmale, B.B. Kale, A.J. Varma, A review on cellulose and lignin based binders and electrodes: Small steps towards a sustainable lithium ion battery, Int. J. Biol. Macromol. 103 (2017) 1032–1043, https://doi.org/10.1016/j.ijbiomac.2017.05.155.
[18] R. Katakojwala, S.V. Mohan, Microcrystalline cellulose production from sugarcane bagasse: Sustainable process development and life cycle assessment, J. Clean. Prod. 249 (2020) 119342, https://doi.org/10.1016/j.jclepro.2019.119342.
[19] S. Kundu, K. Karan, M. Fowler, L.C. Simon, B. Peppley, E. Halliop, Influence of micro-porous layer and operating conditions on the fluoride release rate and degradation of PEMFC membrane electrode assemblies, J. Power Sources 179 (2008) 693–699, https://doi.org/10.1016/j.jpowsour.2007.11.117.
[20] V.O. Mittal, H.R. Kunz, J.M. Fenton, Effect of catalyst properties on membrane degradation rate and the underlying degradation mechanism in PEMFCs, J. Electrochem. Soc. 153 (2006) A1755, https://doi.org/10.1149/1.2219708.
[21] P.C. Okonkwo, I. Ben Belgacem, W. Emori, P.C. Uzoma, Nafion degradation mechanisms in proton exchange membrane fuel cell (PEMFC) system: A review, Int. J. Hydrogen Energy 46 (2021) 27956–27973, https://doi.org/10.1016/j.ijhydene.2021.06.032.
[22] J. Zeng, M.R. Fiorentin, M. Fontana, M. Castellino, F. Risplendi, A. Sacco, G. Cicero, M.A. Farkhondehfal, F. Drago, C.F. Pirri, Novel insights into Sb-cu catalysts for electrochemical reduction of CO2, Appl. Catal. Environ. 306 (2022) 121089, https://doi.org/10.1016/j.apcatb.2022.121089.
[23] J. Zeng, M. Fontana, A. Sacco, D. Sassone, C.F. Pirri, A study of the effect of electrode composition on the electrochemical reduction of CO2, Catal. Today 397 (2022) 463–474, https://doi.org/10.1016/j.cattod.2021.07.014.
[24] J. Zeng, T. Rino, K. Bejtka, M. Castellino, A. Sacco, M.A. Farkhondehfal, A. Chiodoni, F. Drago, C.F. Pirri, et al., ChemSusChem 13 (2020) 4128–4139, https://doi.org/10.1002/cssc.202000971.
[25] J. Zeng, M. Mignosa, N.B.D. Monti, A. Sacco, C.F. Pirri, Engineering copper nanoparticle electrodes for tunable electrochemical reduction of carbon dioxide, Electrochim. Acta 464 (2023) 142862, https://doi.org/10.1016/j.electacta.2023.142862.
[26] Y. Dong, Y. Zhou, Y. Ding, X. Chu, C. Wang, Sensitive detection of Pb(ii) at gold nanoparticle/polyaniline/graphene modified electrode using differential pulse anodic stripping voltammetry, Anal. Methods 6 (2014) 9367–9374, https://doi.org/10.1039/c4ay01908c.
[27] G. Massaglia, V. Margaria, A. Sacco, M. Castellino, A. Chiodoni, F.C. Pirri, M. Quaglio, N-doped carbon nanofibers as catalyst layer at cathode in single chamber microbial fuel cells, Int. J. Hydrogen Energy 44 (2019) 4442–4449, https://doi.org/10.1016/j.ijhydene.2018.10.008.
[28] M. Quaglio, G. Massaglia, N. Vasile, V. Margaria, A. Chiodoni, G.P. Salvador, S. L. Marasso, M. Cocuzza, G. Saracco, F.C. Pirri, A fluid dynamics perspective on material selection in microbial fuel cell-based biosensors, Int. J. Hydrogen Energy 44 (2019) 4533–4542, https://doi.org/10.1016/j.ijhydene.2018.11.087.
[29] V. Mehta, J.S. Cooper, Review and analysis of PEM fuel cell design and manufacturing, J. Power Sources 114 (2003) 32–53, https://doi.org/10.1016/S0378-7753(02)00542-6.
[30] G. Massaglia, T. Serra, F.C. Pirri, M. Quaglio, A nanofiber-based gas diffusion layer for improved performance in air cathode microbial fuel cells, Nanomaterials 13 (2023) 2801, https://doi.org/10.3390/nano13202801.
[31] A.L. Alexe-Ionescu, G. Barbero, L.R. Evangelista, A. Lamberti, A. Pedico, C.F. Pirri, Langmuir adsorption processes and ion transport under bias potential in capacitive deionisation cells, Electrochim. Acta 348 (2020) 136288, https://doi.org/10.1016/j.electacta.2020.136288.
[32] A. Pedico, S. Bocchini, E. Tresso, A. Lamberti, Enhanced capacitive deionization exploiting novel functionalized graphene oxide electrodes, Adv. Mater. Technol. 7 (2022) 2101513, https://doi.org/10.1002/admt.202101513.
[33] B.H. Park, J.H. Choi, Improvement in the capacitance of a carbon electrode prepared using water-soluble polymer binder for a capacitive deionization application, Electrochim. Acta 55 (2010) 2888–2893, https://doi.org/10.1016/j.electacta.2009.12.084.
[34] J. Weng, S. Wang, G. Wang, P. Zhang, B. Lu, H. Wang, J. Jiang, C. Li, Carbon electrode with cross-linked and charged chitosan binder for enhanced capacitive deionization performance, Desalination 505 (2021) 114979, https://doi.org/10.1016/j.desal.2021.114979.
[35] N. Wang, Y. Nuli, S. Su, J. Yang, J. Wang, Effects of binders on the electrochemical performance of rechargeable magnesium batteries, J. Power Sources 341 (2017) 219–229, https://doi.org/10.1016/j.jpowsour.2016.12.003.
[36] H. Wang, B. Wu, X. Wu, Q. Zhuang, T. Liu, Y. Pan, G. Shi, H. Yi, P. Xu, Z. Xiong, S. Chou, B. Wang, Key factors for binders to enhance the electrochemical performance of silicon anodes through molecular design, Small 18 (2021) 2101680, https://doi.org/10.1002/smll.202101680.
[37] E. Pameté, L. Köps, F.A. Kreth, S. Pohlmann, A. Varzi, T. Brousse, A. Balducci, V. Presser, The many deaths of supercapacitors : Degradation, aging, and performance fading, Adv. Energy Mater. 13 (2023) 2301008, https://doi.org/10.1002/aenm.202301008.
[38] J. Lee, K. Sakaushi, M. Antonietti, J. Yuan, Poly(ionic liquid) binders as Li+ conducting mediators for enhanced electrochemical performance, RSC Adv. 5 (2015) 85517–85522, https://doi.org/10.1039/c5ra16535k.
[39] J. Xu, S. Chou, Q. Gu, H. Liu, S. Dou, The effect of different binders on electrochemical properties of LiNi1/3Mn1/3Co1/3O2 cathode material in lithium ion batteries, J. Power Sources 225 (2013) 172–178, https://doi.org/10.1016/j.jpowsour.2012.10.033.
[40] H. Wang, J. Fu, C. Wang, R. Zhang, Y. Yang, Y. Li, C. Li, Q. Sun, H. Li, T. Zhai, A universal aqueous conductive binder for flexible electrodes, Adv. Funct. Mater. 31 (2021) 2102284, https://doi.org/10.1002/adfm.202102284.
[41] Q. Li, M. Kuenzel, J. Wang, T. Diemant, P. Axmann, M. Wohlfahrt-Mehrens, S. Passerini, D. Bresser, Hydroxyethyl cellulose as water-soluble co-binder for cathodes, ChemSusChem (2025) e202500079, https://doi.org/10.1002/cssc.202500079.
[42] Q. Zhang, D. Sun, K. Wang, Z. Ma, T. Xiao, J. Gao, C. Xu, Z. Xiao, X. Ma, Turn the dust into glory: Hierarchical porous carbon cubes derived from waste tire pyrolysis oil exhibits high capability in symmetric capacitors, J. Colloid Interface Sci. 679 (2025) 1219–1230, https://doi.org/10.1016/j.jcis.2024.10.065.
[43] S. Li, Z. Yang, M. Wu, C. Xu, X. Zhang, R. Lin, X. Wang, L. Zhao, D. Sun, X. Ma, J. Gao, Extraordinary compatibility to mass loading and rate capability of hierarchically porous carbon Nanorods electrode derived from the waste Tire pyrolysis oil, Energy Environ. Mater. 5 (2022) 1238–1250, https://doi.org/10.1002/eem2.12240.
[44] S. Darlami, C. Leibing, J. Luis, R. Cid, D. Carriazo, A. Balducci, Brewery waste derived activated carbon for high performance electrochemical capacitors and lithium-ion capacitors, Electrochim. Acta 446 (2023) 142104, https://doi.org/10.1016/j.electacta.2023.142104.
[45] Y. Yang, H. Du, D. Sun, C. Lu, C. Lu, J. Gao, C. Xu, X. Ma, Boosting capacitive performance of S-doped carbon fibers via substrate-oriented activation methodology, Ind. Eng. Chem. Res. 64 (2025) 2745–2757, https://doi.org/10.1021/acs.iecr.4c04038.
[46] M.J. Mostazo-López, R. Ruiz-Rosas, E. Morallón, D. Cazorla-Amorós, Nitrogen doped superporous carbon prepared by a mild method. Enhancement of supercapacitor performance, Int. J. Hydrogen Energy 41 (2016) 19691–19701, https://doi.org/10.1016/j.ijhydene.2016.03.091.
[47] M.J. Mostazo-López, R. Ruiz-Rosas, T. Tagaya, Y. Hatakeyama, S. Shiraishi, E. Morallón, D. Cazorla-Amorós, Nitrogen doped Superactivated carbons prepared at mild conditions as electrodes for supercapacitors in organic electrolyte, C 6 (2020) 56, https://doi.org/10.3390/c6030056.
[48] Y. Yang, H. Du, A. Wang, C. Lu, D. Sun, C. Lu, X. Wang, Z. Xiao, X. Ma, Excellent capacitive storage performance of N-doped porous carbon derived from the orientation-guidance coupled with in-situ activation methodology, J. Colloid Interface Sci. 673 (2024) 657–668, https://doi.org/10.1016/j.jcis.2024.05.237.
[49] M.J. Mostazo-López, D. Salinas-Torres, R. Ruiz-Rosas, E. Morallón, D. Cazorla-Amorós, Nitrogen-doped superporous activated carbons as electrocatalysts for the oxygen reduction reaction, Materials (Basel). 12 (2019) 1346, https://doi.org/10.3390/ma12081346.
[50] X. Ma, Z. Yu, L. Zhao, X. Song, L. Zhao, X. Wang, Z. Xiao, G. Ning, J. Gao, N-doped mesoporous graphene with superior capacitive behaviors derived from chemical vapor deposition methodology in the fluidized bed reactor, Ind. Eng. Chem. Res. 57 (2018) 16327–16334, https://doi.org/10.1021/acs.iecr.8b03498.
[51] T. Tagaya, Y. Hatakeyama, S. Shiraishi, H. Tsukada, M.J. Mostazo-López, E. Morallón, D. Cazorla-Amorós, Nitrogen-doped seamless activated carbon electrode with excellent durability for electric double layer capacitor, J. Electrochem. Soc. 167 (2020) 060523, https://doi.org/10.1149/1945-7111/ab8403.
[52] T. Xiao, Y. Yang, C. Zhang, Y. Li, Q. Zhang, Z. Ma, Q. Xiang, J. Wu, J. Wang, X. Wang, C. Lu, X. Ma, Self-sacrificing template-derived N/O-doped porous carbons: Exceptional capacitor performance across environmental extremes, J. Colloid Interface Sci. 688 (2025) 411–420, https://doi.org/10.1016/j.jcis.2025.02.170.
[53] G. Joshi, V. Rana, S. Naithani, V.K. Varshney, A. Sharma, J.S. Rawat, Chemical modification of waste paper: An optimization towards hydroxypropyl cellulose synthesis, Carbohydr. Polym. 223 (2019) 115082, https://doi.org/10.1016/j.carbpol.2019.115082.
[54] C. Chen, Y. Huang, C. Zhu, Y. Nie, J. Yang, D. Sun, Synthesis and characterization of Hydroxypropyl cellulose from bacterial cellulose, Chinese J. Polym. Sci. (English Ed.) 32 (2014) 439–448, https://doi.org/10.1007/s10118-014-1419-8.
[55] D. Bresser, D. Buchholz, A. Moretti, A. Varzi, S. Passerini, Alternative binders for sustainable electrochemical energy storage – The transition to aqueous electrode processing and bio-derived polymers, Energ. Environ. Sci. (2018), https://doi.org/10.1039/C8EE00640G.
[56] S.F. Lux, F. Schappacher, A. Balducci, S. Passerini, M. Winter, Low cost, environmentally benign binders for Lithium-ion batteries, J. Electrochem. Soc. 157 (2010) A320, https://doi.org/10.1149/1.3291976.
[57] D.L.W. Iii, J. Li, C. Daniel, Prospects for reducing the processing cost of lithium ion batteries, J. Power Sources 275 (2015) 234–242, https://doi.org/10.1016/j.jpowsour.2014.11.019.
[58] M. Valvo, A. Liivat, H. Eriksson, C. Tai, K. Edstrçm, Iron-based electrodes meet water-based preparation, fluorine-free electrolyte and binder : A chance for more sustainable Lithium-ion batteries ? ChemSusChem 10 (2017) 2431–2448, https://doi.org/10.1002/cssc.201700070.

[59] S. Fortin, G. Charlet, Phase diagram of aqueous solutions of (Hydroxypropyl) cellulose, Macromolecules 22 (1989) 2286–2292, https://doi.org/10.1021/ma00195a050.
[60] J. Bajdik, G. Regdon Jr., T. Marek, I. Eros, K. Suvegh, K. Pintye-Hòdi, The effect of the solvent on the film-forming parameters of, Int. J. Pharm. 301 (2005) 192–198, https://doi.org/10.1016/j.ijpharm.2005.05.031.
[61] M.J. Hey, D.P. Jackson, H. Yan, The salting-out effect and phase separation in aqueous solutions of electrolytes and poly (ethylene glycol), Polymer (Guildf). 46 (2005) 2567–2572, https://doi.org/10.1016/j.polymer.2005.02.019.
[62] P. Ruschhaupt, A. Varzi, S. Passerini, Natural polymers as green binders for high-loading supercapacitor electrodes, ChemSusChem 13 (2020) 763–770, https://doi.org/10.1002/cssc.201902863.
[63] A. Scalia, P. Zaccagnini, M. Armandi, G. Latini, D. Versaci, V. Lanzio, A. Varzi, S. Passerini, A. Lamberti, Tragacanth gum as green binder for sustainable water-Processable electrochemical capacitor, ChemSusChem 13 (2020) 1–8, https://doi.org/10.1002/cssc.202001754.
[64] D. Versaci, R. Nasi, U. Zubair, J. Amici, M. Sgroi, M.A. Dumitrescu, C. Francia, S. Bodoardo, N. Penazzi, New eco-friendly low-cost binders for Li-ion anodes, J. Solid State Electrochem. 21 (2017) 3429–3435, https://doi.org/10.1007/s10008-017-3665-5.
[65] D. Bresser, D. Buchholz, A. Moretti, A. Varzi, S. Passerini, Alternative binders for sustainable electrochemical energy storage-the transition to aqueous electrode processing and bio-derived polymers, Energ. Environ. Sci. 11 (2018) 3096–3127, https://doi.org/10.1039/c8ee00640g.
[66] K. Sun, T. Wei, B.Y. Ahn, J.Y. Seo, S.J. Dillon, J.A. Lewis, 3D printing of interdigitated Li-ion microbattery architectures, Adv. Mater. 25 (2013) 4539–4543, https://doi.org/10.1002/adma.201301036.
[67] K. Sun, C.A. Cama, J. Huang, Q. Zhang, S. Hwang, D. Su, A.C. Marschilok, K. J. Takeuchi, E.S. Takeuchi, H. Gan, Effect of carbon and binder on high sulfur loading electrode for Li-S battery technology, Electrochim. Acta 235 (2017) 399–408, https://doi.org/10.1016/j.electacta.2017.03.023.
[68] B. Yao, S. Chandrasekaran, J. Zhang, W. Xiao, F. Qian, C. Zhu, E.B. Duoss, C. M. Spadaccini, M.A. Worsley, Y. Li, Efficient 3D printed Pseudocapacitive electrodes with ultrahigh MnO 2 loading, Joule 3 (2019) 459–470, https://doi.org/10.1016/j.joule.2018.09.020.
[69] L. Bargnesi, A. Rozzarin, G. Lacarbonara, S. Tombolesi, C. Arbizzani, Sustainable modification of chitosan binder for capacitive electrodes operating in aqueous electrolytes, ChemElectroChem 10 (2023) 1–8, https://doi.org/10.1002/celc.202201080.
[70] Y. Ding, X. Zhong, C. Yuan, L. Duan, L. Zhang, Z. Wang, C. Wang, F. Shi, Sodium Alginate Binders for Bivalency Aqueous Batteries (2021), https://doi.org/10.1021/acsami.1c02995.
[71] G. Landi, L. La Notte, A.L. Palma, A. Sorrentino, M.G. Maglione, G. Puglisi, A comparative evaluation of sustainable binders for environmentally friendly carbon-based supercapacitors, Nanomaterials (2022), https://doi.org/10.3390/nano12010046.
[72] X. Hu, A.K.J. An, S.S. Chopra, Life Cycle Assessment of the Polyvinylidene Fluoride Polymer with Applications in Various Emerging Technologies (2022), https://doi.org/10.1021/acssuschemeng.1c05350.
[73] M. Gornik, Methyl Cellulose LCA. https://www.epd-norge.no/getfile.php/13162458-1741628810/EPDer/Kjemikalier/NEPD-5642-4909_Methylcellulose-.pdf, 2024.
[74] H.D. Abruña, M.A. Lowe, P.-L. Taberna, B. Dunn, V. Augustyn, S.H. Tolbert, J. W. Kim, J. Come, P. Simon, High-rate electrochemical energy storage through Li+ intercalation pseudocapacitance, Nat. Mater. 12 (2013) 518–522, https://doi.org/10.1038/nmat3601.
[75] S.I. Cheong, B. Kim, H. Lee, J.W. Rhim, Physical adsorption of water-soluble polymers on hydrophobic polymeric membrane surfaces via salting-out effect, Macromol. Res. 21 (2013) 629–635, https://doi.org/10.1007/s13233-013-1075-9.
[76] P. Azaïs, L. Duclaux, P. Florian, D. Massiot, M.A. Lillo-Rodenas, A. Linares-Solano, J.P. Peres, C. Jehoulet, F. Béguin, Causes of supercapacitors ageing in organic electrolyte, J. Power Sources 171 (2007) 1046–1053, https://doi.org/10.1016/j.jpowsour.2007.07.001.
[77] Q. Abbas, D. Pajak, Effect of binder on the performance of carbon/carbon symmetric capacitors in salt aqueous electrolyte, Electrochim. Acta 140 (2014) 132–138, https://doi.org/10.1016/j.electacta.2014.04.096.
[78] B. Xu, H. Wang, Q. Zhu, N. Sun, B. Anasori, L. Hu, F. Wang, Reduced graphene oxide as a multi-functional conductive binder for supercapacitor electrodes, Energy Storage Mater. 12 (2018) 128–136, https://doi.org/10.1016/j.ensm.2017.12.006.
[79] O.W. Guirguis, M.T.H. Moselhey, Thermal and structural studies of poly (vinyl alcohol) and hydroxypropyl cellulose blends 4 (2012) 57–67, https://doi.org/10.4236/ns.2012.41009.
[80] 2025 NIST - Dimethyl Sulfoxide CAS: 67-68-5 accessed January 30, Dimethyl Sulfoxide CAS: 67-68-5 accessed January 30, 2025, Chem. Webb. (2025) 3–5. https://webbook.nist.gov/cgi/cbook.cgi?ID=C67685&Type=IR-SPEC&Index=0#IR-SPEC.
[81] T. Nguyen, Degradation of poly[vinyl fluoride] and poly[vinylidene fluoride], J. Macromol. Sci. Part C Polym. Rev. (1985) 227–275, https://doi.org/10.1080/15583728509412823.
[82] 2025 NIST - Ethene, fluoro- CAS: 75-02-5 accessed January 30, Ethene, fluoro- CAS: 75-02-5 accessed January 30, 2025, Chem. Webb. (2025) 30–31. https://webbook.nist.gov/cgi/cbook.cgi?ID=C75025&Units=SI&Mask=80#IR-Spec.
[83] 2025 NIST - Propanal CAS: 123-38-6 accessed January 30, Propanal CAS: 123-38-6 accessed January 30, 2025, Chem. Webb. (2025) 6–8. https://webbook.nist.gov/cgi/cbook.cgi?ID=C123386&Type=IR-SPEC&Index=0.
[84] 2025 NIST - Acetone CAS: 67-64-1 accessed January 30, Acetone CAS: 67-64-1 accessed January 30, 2025, Chem. Webb. (2025) 3–5. https://webbook.nist.gov/cgi/cbook.cgi?ID=C67641&Type=IR-SPEC&Index=0.
[85] S. Dsoke, X. Tian, C. Täubert, S. Schlüter, M. Wohlfahrt-Mehrens, Strategies to reduce the resistance sources on electrochemical double layer capacitor electrodes, J. Power Sources 238 (2013) 422–429, https://doi.org/10.1016/j.jpowsour.2013.04.031.
[86] L. Kops, P. Zaccagnini, C. Fabrizio, A. Balducci, Determination of reliable resistance values for electrical double-layer capacitors, J. Power Sources Adv. 16 (2022) 100098, https://doi.org/10.1016/j.powera.2022.100098.
[87] M.J. Lacey, F. Jeschull, K. Edström, D. Brandell, Porosity blocking in highly porous carbon black by PVdF binder and its implications for the Li-S system, J. Phys. Chem. C 118 (2014) 25890–25898, https://doi.org/10.1021/jp508137m.
[88] S.W. Seo, W.J. Ahn, Y.S. Lee, S.C. Kang, J.S. Im, Improvement of capacitor performance by pitch-based binder for a new alternative to polymer binders, Surfaces and Interfaces. 37 (2023) 102726, https://doi.org/10.1016/j.surfin.2023.102726.
[89] J. Krjka, R. Mrfiz, I. Rouk, Corrosion rate of titanium in H2S04, Mater. Chem. Phys. 48 (1997) 64–67, https://doi.org/10.1016/S0254-0584(97)80079-X.
[90] B.E. Conway, Electrochemical Supercapacitors (1999), https://doi.org/10.1007/978-1-4757-3058-6_10.
[91] M. Aslan, D. Weingarth, P. Herbeck-Engel, I. Grobelsek, V. Presser, Polyvinylpyrrolidone/polyvinyl butyral composite as a stable binder for castable supercapacitor electrodes in aqueous electrolytes, J. Power Sources 279 (2015) 323–333, https://doi.org/10.1016/j.jpowsour.2014.12.151.
[92] W. Zhu, K. Okada, Z. Li, J. Zhu, E. Marin, G. Pezzotti, Effect of component content variation on composition and structure of activated carbon in PVDF:K2CO3, Phys. Chem. Chem. Phys. 21 (2019) 2382–2388, https://doi.org/10.1039/c8cp06503a.